

Coherence-enhanced imaging of a degenerate Bose gas

L. E. Sadler, J. M. Higbie, S. R. Leslie, M. Vengalattore, and D. M. Stamper-Kum
Department of Physics, University of California, Berkeley CA 94720
(dated: December 29, 2021)

We present coherence-enhanced imaging, an in situ technique that uses Raman superradiance to probe the spatial coherence properties of an ultracold gas. Applying this method, we obtain a spatially resolved measurement of the condensate number and more generally, of the first-order spatial correlation function in a gas of ^{87}Rb atoms. We observe the enhanced decay of propagating spin gratings in high density regions of a Bose condensate, a decay we ascribe to collective, non-linear atom-atom scattering. Further, we directly observe spatial inhomogeneities that arise generally in the course of extended sample superradiance.

PACS numbers: 03.75.+b, 42.50.Ct, 42.50.Gy

Ultracold Bose and Fermi gases represent new condensed-matter systems in which to study the conditions for and onset of long-range off-diagonal order [1]. Beyond serving as models of existing quantum fluids, gaseous systems allow for studies of coherent matter far from equilibrium. Studying such non-equilibrium samples may yield insights into symmetry-breaking dynamics at thermal and quantum phase transitions [2, 3, 4]. A direct probe of off-diagonal order in these dilute gases is essential to fully exploit this opportunity.

Limitations of existing techniques for measuring coherence have narrowed the scope of prior studies. In time-of-flight methods, coherence is detected through matter-wave interference, which provides poor spatial resolution. This reduced resolution may preclude studying coherence in inhomogeneous systems such as at the borders of Mott-insulating regions of bosons in optical lattices [5], gases trapped in disordered potentials [6], or systems undergoing a first-order phase transition to a superfluid state [7, 8, 9, 10]. A second technique, the imaging of irrotational flow as a signal for phase coherence, requires the gaseous system to be strongly perturbed over extended periods of time. This agitation prevents direct measurements of phase coherence in rapidly evolving systems or in systems near a phase transition.

In this Letter, we describe coherence-enhanced imaging, which allows the coherent portions of a gaseous system to be directly identified with high spatial resolution. Previous in situ imaging methods [11, 12, 13], being sensitive to the linear optical susceptibility of the trapped gas, allow the identification of the coherent portion of the gas only through its high optical density. In contrast, our imaging method relies on a non-linear optical property of the trapped gas, superradiance-enhanced absorption, to gain access to the difference in coherence between the condensed and non-condensed portions of the gas.

We present two main results derived from coherence-enhanced images. First, we quantify coherence properties in a degenerate ^{87}Rb gas. Specifically, we obtain a spatially resolved measure of the condensate number without resorting to model-dependent fitting of spatial images [14]. We measure the first-order spatial correlation function in a partly condensed gas with high spatial

resolution. Second, we obtain the first spatially and temporally resolved study of extended sample superradiance, revealing inhomogeneous collective scattering across the gas.

Collective light scattering has been observed in many systems including solid crystals [15], plasmas [16], and gases [17]. Such scattering can be regarded as a form of extended-sample superradiance [18] where the pump light that illuminates the sample places all scatterers into an excited state from which they may optically decay. The light emitted from these systems is highly directed and is the primary signal used to study the temporal evolution of this process. An additional signature of superradiance in ultracold gases is the directed emission of atoms from the original atomic sample following the momentum recoil from superradiant light emission [19]. Here we focus on a new signature of superradiance, namely the enhanced absorption of the pump light due to collectively enhanced light scattering. Imaging this light yields detailed spatial information on the radiating sample.

Spontaneous collective light scattering is most easily described in the context of Rayleigh superradiance. In this process, off-resonant light pumps atoms to an excited state whence they decay, recoiling with momentum $\sim \mathbf{q} = \mathbf{k}_i - \mathbf{k}_s$ which is the difference between the momentum of the incident and scattered photons. Spatial coherence between the recoiling and stationary atoms causes a periodic density grating to form through matter-wave interference. This density grating acts as a partially reflective mirror, oriented so as to scatter light in the same direction as previously scattered light, and the reflectivity of which is proportional to the local density of unscattered and scattered atoms. In a prolate sample, the enhanced light scattering is directed predominantly along the end modes (EFM), i.e. along the long axis of the gas. The mechanism for Raman superradiance, which is used in this work, differs in that interference between recoiling and stationary atoms creates a spin-polarization rather than a number-density grating and in that recoiling atoms no longer scatter light [20, 21].

The enhancement of the optical scattering rate depends solely on the quality of the grating formed in the gas. In turn, properties of the grating depend on the

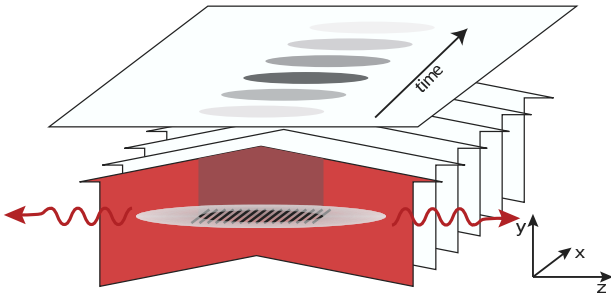


FIG. 1: Experimental scheme for coherence-enhanced imaging. Short-pulses of light illuminate a prolate gas perpendicular to the magnetic field axis (\hat{z}). Superradiance establishes a coherent polarization grating in spatially coherent portions of the gas, causing collective absorption of probe light and its re-emission along the end-remodes. Each incident pulse is imaged separately, yielding images such as shown in Figure 2.

competition between a position-dependent loss of grating coherence and the amplification of the grating by stimulated emission. The loss of grating coherence can occur due to Doppler dephasing or collisional dephasing and loss. Considering just Doppler dephasing, the polarization grating formed by the unscattered and re-coiling atoms will decay on a timescale $\tau_c \sim (\hbar/qv)^{-1}$ with v being the local atomic rms velocity. This correlation time, τ_c , is the time it takes atoms propagating at momentum $\hbar q$ to travel beyond the coherence length $\lambda_c \sim \hbar/mv$, with m being the atomic mass. As a result, polarization gratings in gases with long coherence lengths, such as a Bose-Einstein condensate (BEC), persist much longer than those in non-degenerate gases with short, temperature (T) dependent coherence lengths $\tau_{dB} \sim \frac{\hbar}{2\sqrt{2}m k_B T}$.

In our experiment, we induce superradiance in a gas using multiple, short pulses of light separated by a variable delay time τ_d . Enhanced absorption, which we image, is built up over multiple pulses in the portion of the gas with $\tau_c > \tau_d$, while Doppler dephasing in the portion of the sample with $\tau_c < \tau_d$ suppresses the pulse-to-pulse growth of the polarization grating. Our imaging method provides a spatially resolved measure of the first-order spatial correlation function. That is, an optical absorption signal is obtained that quantifies the modulation depth of interference between the stationary gas and its replica, displaced by $r = \hbar q/m$.

Our experiments were performed on anisotropic (cigar-shaped) gases of ^{87}Rb trapped in a Ioffe-Pritchard magnetic trap in the $F = 1; m_F = -1$ hyperfine state. The magnetic trap was characterized by trap frequencies of $\omega_{x,y,z} = 2(48; 48; 5) \text{ s}^{-1}$ in the transverse (\hat{x}, \hat{y}) and axial (\hat{z}) directions. The gas temperature was varied by the final settings used in rf evaporative cooling, yielding gases of 15×10^6 atoms at the BEC transition temperature of 250 nK, and pure condensates of up to 1.6×10^6 atoms.

The light used for superradiance-enhanced imaging

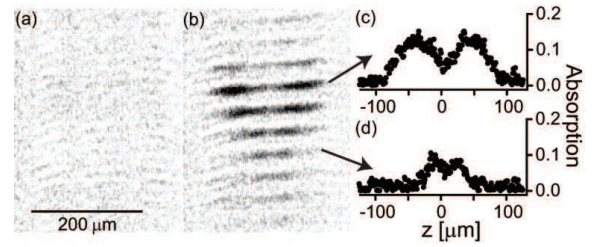


FIG. 2: Direct, in situ imaging of coherence in a BEC. Coherence-enhanced absorption images are shown for single trapped Bose gases at (a) $T = T_c = 1.3$ and (b) $T = T_c = 0.3$. Each of ten frames is illuminated by a 100 μs pulse of light separated by $\tau_d = 68 \mu\text{s}$ delay times and is shown with time evolving from the top to the bottom frame. Doppler dephasing during the delay times suppresses superradiance except in coherent portions of the gas. Thus, enhanced absorption is seen only in the condensed portions of the degenerate sample (b). The absorption signal varies across the cloud with collective enhancement occurring first at the ends of the extended sample.

was directed along the \hat{y} axis, linearly polarized perpendicular to the \hat{z} magnetic field axis (Fig. 1), and detuned by 102 MHz above the $F = 1 \rightarrow F' = 1$ D1 transition ($k_i = 2\pi/795 \text{ nm}$). This detuning and polarization was chosen for two reasons. First, Rayleigh scattering is eliminated due to destructive interference among the transitions to the $F' = 1$ and the $F' = 2$ excited hyperfine states. This eliminates the dispersive phase shift that would otherwise cause aberrations in imaging the $10 \mu\text{m}$ narrow cloud. Second, at this detuning, effects on collective light scattering from both Zeeman and mean-field interaction shifts are made negligible due to a predominant superradiant scattering to the $F' = 2; m_F = 1$ hyperfine state. This final state possesses a nearly equal magnetic moment to the initial state, and the relative s-wave scattering lengths among all trapped states are nearly identical.

Coherence-enhanced images of a pure condensate taken at this detuning (Fig. 2) demonstrate the spatial and temporal resolution of our technique. For these images, a BEC of 1.6×10^6 atoms was illuminated by a series of 100 μs -long pulses of light, with a $\tau_d = 68 \mu\text{s}$ delay between pulses. The transmitted part of each probe pulse was separately imaged at a diffraction-limited resolution of $\sim 6 \mu\text{m}$. The absorption by the condensate increases over several probe pulses due to the collective Raman scattering culminating in a peak absorption of 15%. After achieving maximum enhancement, the absorption diminishes as a large fraction of the condensed atoms have been optically pumped to the $F' = 2; m_F = 1$ state in which they no longer absorb probe light.

To estimate the maximum absorption expected for this sample, let us consider superradiant scattering solely into one EFM and into one final atomic state ($F' = 2; m_F = 1$). In the case when half the atoms have been scattered and presuming simultaneous collective behavior by

all atoms in the sample, the optical depth is enhanced by a factor $E = \frac{R_j - f_j}{R_{\text{tot}}} N_0 A$. Here, $R_j = R_{\text{tot}} = 0.28$ is the branching ratio for scattering into the preferred final state $|j\rangle$, f_j is an angular term that includes the dipole emission pattern, N_0 is the total atom number, and A is a phase-matching integral [19]; here $N_0 A = 5800$. We thus predict a maximum enhancement factor $E \sim 60$, somewhat greater than the observed $E \sim 10$.

This discrepancy in enhancement is not surprising given the significant spatial features seen in the coherence-enhanced images (Fig. 2). These images show a distinctive pattern in which the ends of the extended sample darken earlier than the denser cloud center. Thus, the maximum enhancement of light scattering does not occur simultaneously throughout the cloud, diminishing the overall enhancement of absorption as compared with the estimate described above. This diminished enhancement is most pronounced at the center of the gas because the majority of atoms in the sample have been transferred to the recoiling state, diminishing the depth of the grating from which light is scattered.

Extensions to the simplest superradiance models have been constructed [22, 23] that predict the spatial inhomogeneities that we observe. In these models, the initiation of collective scattering is treated in a manner akin to Dicke's original work [18] in which light scattering leads to the occupation of atomic recoil modes that are propagating replicas of the unscattered atomic state. Once collective scattering dominates, subsequent developments are described semi-classically. Here, light propagating down the long axis of the sample acquires its highest intensity at the tip of the gas. Atoms located at the tips are thus more strongly stimulated by the field and emit light earlier than those in the center of the cloud. While the development of spatial structure was indicated indirectly by previous studies [24, 25], coherence-enhanced imaging gives unprecedented temporal and spatial resolution of the entire superradiant process.

Beyond providing insight on the dynamics of superradiance, these multiple-frame images yield quantitative information about spatial coherence in trapped gases. For example, in contrast with linear absorption imaging, coherence-enhanced imaging allows the coherent fraction of the partially condensed Bose gas to be spatially mapped and its population counted. Images obtained by each of these methods are compared in Fig. 3. The off-resonant linear absorption images, taken with light 200 MHz below the $D_2 F=1 \rightarrow F=2$ transition to eliminate dispersive phase shifts, show a typical progression of density distributions from Gaussian for $T=T_c > 1$, to bimodal, and finally to a single parabolic (condensate) density distribution for the smallest $T=T_c$. In contrast, coherence-enhanced absorption appears only when $T=T_c < 1$. Here, we present maps, derived from multiple-frame images such as those in Fig. 2, that give the net coherence-enhanced absorption, i.e. each map pixel shows the total number of missing probe photons summed over all image frames. Coherence-enhanced imaging selec-

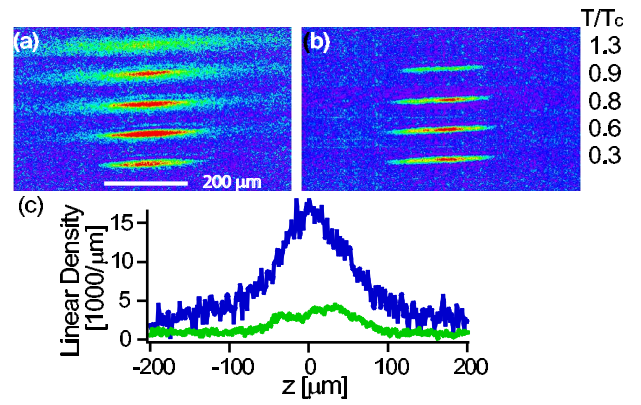


FIG. 3: Spatial maps of condensate number. (a) Dispersion-free off-resonant linear absorption images are given for varying $T=T_c$ revealing the combined densities of the condensed and normal fractions of the gas, while providing no direct information on its coherence. (b) Coherence-enhanced images, derived from collating many frames from a multiple-pulse imaging sequence, exclusively reveal portions of the gas that are phase-coherent. (c) Radially summed (across x) cross-section for a gas at $T=T_c=0.9$ shows a bimodal (blue) total number distribution in linear absorption imaging and condensate-only distribution (green) in coherence-enhanced images, which is 25% of the total number.

tively resolves the condensed portion of the gas, whereas this portion is obscured in the linear absorption images. Under the assumption that the condensate is completely optically pumped to the $F=2; m_F=1$ state during multiple-pulse superradiance, the number of missing photons directly quantifies the condensate number.

Moreover, by varying the delay times in our imaging sequence, we obtain a spatially resolved measurement of the first order spatial correlation function. For this purpose, we determine, at each pixel location, the ratio of absorption between the first and second frame in the image. This technique, similar to that of Ref. [25] in which the ratio of superradiant light emission intensities was considered, measures the spatial correlations between atoms at varying distances, $r = \sim q = m$. The absorption ratio, which measures the overlap of the recoiling and stationary spatial wavefunctions, is large in portions of the gas with high spatial coherence and tends to unity when the correlations being probed exceed the local coherence length.

Multiple-pulse coherence-enhanced images were taken of identically prepared gaseous samples with variable delay times. In Fig. 4 we present maps of the characteristic coherence time $\tau_c(x; z)$, which we obtain at each pixel as the $1/e$ decay time of the absorption ratio as determined by Gaussian fits. We observe a maximum coherence time, $\tau_c = 1.6$ ms, which is consistent with the time required for recoiling atoms to travel through the condensate. This shows that BECs are coherent across their radial width as previously seen in Ref. [26, 27, 28].

Surprisingly, however, we find that τ_c diminishes in

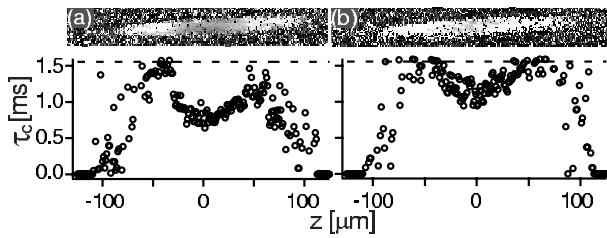


FIG. 4: Maps of correlation times $\tau_c(x; z)$ shown for degenerate Bose gases at (a) $T=T_c = 0.3$ and (b) $T=T_c = 0.8$. Longitudinal cross-sections are shown below the corresponding images. The Doppler limit on the correlation time (dashed line) matches measurement at the least dense but fully coherent tips of the condensate. The reduction of τ_c at the condensate center is ascribed to non-linear atom-atom elastic scattering. Gray scale runs from 0 to 1.6 m s.

the center of the BEC, most dramatically for samples at the lowest temperatures at which the condensate fraction and density are the highest. Rather than taking this observation to imply a reduced spatial coherence at the center of the condensate, we ascribe the lowering of τ_c to non-linear collisional depletion of the propagating spin grating formed in superradiance [29]. The linear (non-collective) per-particle scattering rate of atoms recoiling at v_{rec} propagating through the stationary portion of the gas, $\Gamma_1 = n v_{\text{rec}} = 300 \text{ s}^{-1}$ is too small to significantly affect the observed correlation times. However, in a coherent gas, such scattering is enhanced to the extent that the total number of collisions, N_s exceeds the number of quantum states M available to the collision products. We estimate the enhanced non-linear scattering rate in a volume with a radius that is equal to the distance the sample recoils before the grating decays to be $\Gamma_{\text{nl}} = \frac{1}{2} (v_{\text{rec}}^2 n_s) = 6 \times 1/(500 \text{ s})$ where $v_{\text{rec}} = 795 \text{ nm/s}$ and n_s is the density of the scattered

atoms. This rate is in good agreement with the value of τ_c observed at the center of the condensate. In more dilute regions, such as the tips of the condensate, or in the center of less dense condensate formed at higher temperatures, the collective enhancement of collisional losses is weaker, and thus, higher values of τ_c are observed.

As we have shown, coherence-enhanced imaging yields simultaneous information both on the spatial coherence of an ultracold gas and also on superradiance in extended samples. Quantitative measures of the first-order spatial correlation function were obtained at high spatial resolution over the extent of the gas. However, the spatial structures seen to appear in the course of superradiance are an inconvenient feature that complicate the analysis. Alternatively, one could employ a two-photon stimulated Raman transition to set up the initial, now uniform, polarization grating, and then image the collectively enhanced absorption of a subsequent single probe beam. Such an approach is technically complicated by the need for two laser beams with a precise frequency difference and also by sensitivity to overall Doppler shifts for a possibly moving gas sample. Our method avoids such complications.

On the other hand, coherence-enhanced imaging as implemented here has allowed for the first direct temporal and spatial study of the onset of inhomogeneous collective scattering and offers avenues to further study. As pointed out recently [23], fluctuating asymmetries in the spatial structure that develop spontaneously during superradiance may be studied to characterize further the quantum fluctuations that play a role in its early stages.

We thank P. M. Eystre and H. Uys for discussions and D. Schneble for comments on the manuscript. This work was supported by the NSF and the David and Lucile Packard Foundation. S.R.L. acknowledges support from the NSERC.

-
- [1] M. Greiner et al, Nature 415, 39 (2002).
 [2] W. H. Zurek et al, Phys. Rev. Lett. 95, 105701 (2005).
 [3] T. W. B. Kibble, J. Phys. A 9, 1387 (1976).
 [4] W. H. Zurek, Nature 317, 505 (1985).
 [5] D. Jaksch et al, Phys. Rev. Lett. 81, 3108 (1998).
 [6] J. E. Lye et al, Phys. Rev. Lett. 95, 070401 (2005).
 [7] E. Altman et al, New Journal of Physics 5, 113 (2003).
 [8] K. V. Knutitsky and R. Graham, Phys. Rev. A 70, 636101 (2004).
 [9] A. Kuklov et al, Phys. Rev. Lett. 93, 230402 (2004).
 [10] T. Kinoshita et al, Phys. Rev. Lett. 94, 110403 (2005).
 [11] M. R. Andrews et al, Science 273, 84 (1996).
 [12] M. R. Andrews et al, Phys. Rev. Lett. 79, 553 (1997).
 [13] L. V. Hau et al, Phys. Rev. A 58, R54 (1998).
 [14] W. Ketterle et al, in Bose-Einstein condensation in atomic gases, edited by M. Inguscio, S. Stringari, and C. Wieman (IOS Press, Amsterdam, 1999), Proceedings of the International School of Physics "Enrico Fermi," Course CXL, pp. 67-176.
 [15] R. Florian et al, Phys. Rev. A 29, 2709 (1984).
 [16] M. Decher et al, Phys. Rev. Lett. 93, 095001 (2004).
 [17] N. Skribanowitz et al, Phys. Rev. Lett. 30, 309 (1973).
 [18] R. H. Dicke, Phys. Rev. 93, 99 (1954).
 [19] S. Inouye et al, Science 285, 571 (1999).
 [20] D. Schneble et al, Phys. Rev. A 69, 041601(R) (2004).
 [21] Y. Yoshikawa et al, Phys. Rev. A 69, 041603(R) (2004).
 [22] J. C. McGillivray and M. S. Feld, Phys. Rev. A 14, 1169 (1976).
 [23] H. Uys and P. M. Eystre, preprint arXiv:cond-mat/0602343 v2.
 [24] D. Schneble et al, Science 300, 475 (2003).
 [25] Y. Yoshikawa et al, Phys. Rev. Lett. 94, 083602 (2005).
 [26] M. R. Andrews et al, Science 275, 637 (1997).
 [27] J. Stenger et al, Phys. Rev. Lett. 82, 4569 (1999).
 [28] E. W. Hagley et al, Phys. Rev. Lett. 83, 2113 (1999).
 [29] A. C. Chikkatur et al, Phys. Rev. Lett. 85, 483 (2000).